Metformin promotes lifespan through mitohormesis via the peroxiredoxin PRDX-2

Wouter De Haes[a], Lotte Frooninckx[a], Roel Van Assche[a], Arne Smolders[b], Geert Depuydt[a], Johan Billen[c], Bart P. Braeckman[b], Liliane Schoofs[a,1], and Liesbet Temmerman[a]

[a]Laboratory for Functional Genomics and Proteomics and [c]Laboratory of Socioecology and Social Evolution, Department of Biology, KU Leuven, 3000 Leuven, Belgium; and [b]Laboratory for Aging Physiology and Molecular Evolution, Department of Biology, Ghent University, 9000 Ghent, Belgium

Edited by Andy Dillin, University of California, Berkeley, CA, and accepted by the Editorial Board April 28, 2014 (received for review November 28, 2013)

The antiglycemic drug metformin, widely prescribed as first-line treatment of type II diabetes mellitus, has lifespan-extending properties. Precisely how this is achieved remains unclear. Via a quantitative proteomics approach using the model organism *Caenorhabditis elegans*, we gained molecular understanding of the physiological changes elicited by metformin exposure, including changes in branched-chain amino acid catabolism and cuticle maintenance. We show that metformin extends lifespan through the process of mitohormesis and propose a signaling cascade in which metformin-induced production of reactive oxygen species increases overall life expectancy. We further address an important issue in aging research, wherein so far, the key molecular link that translates the reactive oxygen species signal into a prolongevity cue remained elusive. We show that this beneficial signal of the mitohormetic pathway is propagated by the peroxiredoxin PRDX-2. Because of its evolutionary conservation, peroxiredoxin signaling might underlie a general principle of prolongevity signaling.

Metformin, an antiglycemic biguanide drug and the most common treatment of type II diabetes mellitus, has life-extending capabilities (1, 2). Several other human diseases, such as cancer (3) and nonalcoholic fatty liver disease (4), are also potentially alleviated by metformin treatment. This suggests that metformin acts on common pathways involved in a spectrum of aging-related disorders. Because of its demonstrated beneficial effect on lifespan in the nematode *Caenorhabditis elegans* (5, 6) and in the rodents *Rattus norvegicus* (1) and *Mus musculus* (2), these models facilitate research into the underlying mode of action.

It has been hypothesized that metformin elicits its beneficial effects by mimicking dietary restriction (DR) (7), a regimen wherein a physiological response is triggered by reducing the uptake of nutritive calories. The physiological response to DR causes lifespan extension and delays age-dependent decline from yeast to primates (8). The idea of similarity sprouts from the observed low blood glucose and insulin levels combined with increased glucose utilization in both calorically restricted and metformin-treated animals (7). In addition, metformin-treated worms show phenotypes similar to DR worms (5), and transcript profiles of metformin-treated and DR mice also overlap significantly (9).

Caution is due, however, in referring to DR, because different methods to induce DR in *C. elegans* act through different genes to elicit corresponding effects on lifespan (10–12). Glucose restriction, a specific type of DR, requires AMP-dependent kinase (AMPK) to extend lifespan. Activation of AMPK leads to increased mitochondrial production of reactive oxygen species (ROS), which induces stress defense and results in a net increase in longevity. This process of lifespan extension based on mitochondrial oxidative stress is known as mitohormesis (13).

Despite its similarities to DR and its widespread use as an antiglycemic drug, the actual mode of action of metformin is largely unknown and a subject of much debate. In mammals, metformin is generally believed to act through the activation of AMPK, one of the main regulators of cellular energy homeostasis (2, 14–16), but recent research suggests the existence of AMPK-independent mechanisms as well (17, 18). More upstream, metformin is thought to activate AMPK through partial inhibition of complex I of the electron transport chain (ETC) and a resultant increase in the AMP/ATP ratio (19–21), although again, not all data support this theory (16, 22). Important players in metformin-induced lifespan extension in *C. elegans* are the liver kinase B1 ortholog PAR-4, the AMPK ortholog AMP-activated kinase-2 (AAK-2), and the skinhead-1 (SKN-1) transcription factor, which is involved in activating phase II detoxification mechanisms (5). It has recently been demonstrated that in *C. elegans*, metformin partly elicits its effects through altering the folate metabolism of its microbial food source (6), but questions about its direct effects are largely unaddressed. It is, for instance, unclear how metformin induces AAK-2 and SKN-1 activity. Overall, many gaps remain in our knowledge of metformin-induced lifespan extension.

To study the targets of metformin, we performed a proteomic analysis on metformin-treated *C. elegans* and used the results as a framework for follow-up experiments. We observed striking similarities between metformin-treated and glucose-restricted worms and discovered several factors involved in mitohormetic regulation of lifespan, including a previously unidentified role for peroxiredoxin-2 (PRDX-2), which seems to be responsible for translating oxidative stress into a downstream prolongevity signal. In addition to lifespan extension, we also report features that contribute to the healthspan of metformin-treated worms.

Significance

Recently it has been suggested that metformin, the most commonly used antidiabetic drug, might also possess general health-promoting properties. Elucidating metformin's mode of action will vastly increase its application range and will contribute to healthy aging. We reveal a signaling cascade in which metformin is able to extend lifespan by increasing the production of reactive oxygen species (ROS). This allowed us to further work at the crossroads of human disease and aging research, identifying a key molecule that is able to translate the ROS signal into a prolongevity cue: an antioxidant peroxiredoxin is also able to activate a lifespan-promoting signaling cascade, here described in detail. Continued research efforts in this field lead toward a targeted improvement of aging-related complications.

Author contributions: W.D.H., B.P.B., L.S., and L.T. designed research; W.D.H., L.F., R.V.A., A.S., G.D., and J.B. performed research; W.D.H., L.F., R.V.A., A.S., and G.D. analyzed data; and W.D.H. and L.T. wrote the paper.

The authors declare no conflict of interest.

This article is a PNAS Direct Submission. A.D. is a guest editor invited by the Editorial Board.

Freely available online through the PNAS open access option.

[1]To whom correspondence should be addressed. E-mail: Liliane.Schoofs@bio.kuleuven.be.

This article contains supporting information online at www.pnas.org/lookup/suppl/doi:10.1073/pnas.1321776111/-/DCSupplemental.

Results

Molecular Changes in *Caenorhabditis elegans* upon Metformin Exposure: A Proteomic Approach. To gain a deeper understanding of the physiological changes elicited by metformin exposure, a differential gel-based proteomics experiment was performed. A total of 164 spots with differential abundances were detected, 134 of which could be identified by mass spectrometry. After removal of duplicate identifications, the final analysis resulted in a list of 58 up-regulated and 30 down-regulated proteins (Dataset S1).

Enrichment analysis (23) of the up-regulated proteins resulted in the detection of several overrepresented pathways (Table 1), of which the branched-chain amino acid (BCAA) degradation pathway was most markedly enriched. All other enriched pathways, including glycolysis and the tricarboxylic acid (TCA) cycle, are involved in general energy metabolism. No significant pathway enrichment was observed in the analysis of down-regulated proteins. Combined analysis of all differential proteins (both up and down) did not reveal additional pathways of interest.

Further functional clustering was used to subdivide the up- and down-regulated proteins into meaningful groups (Table 1). For each functional cluster detailed information, including subterms and proteins in each group, was gathered to assist in data interpretation (Dataset S1). These results were used as the backbone of hypothesis-driven experiments into the mechanisms induced by metformin treatment.

Table 1. Functional analysis of differential proteins

Pathway or cluster affected by metformin	Significance value
Pathway enrichment of up-regulated proteins*	
Pathway	*P* value
Valine, leucine, and isoleucine degradation	9.85E-09
Citrate cycle (TCA cycle)	1.38E-04
Glycolysis/gluconeogenesis	2.47E-04
Pyruvate metabolism	4.62E-04
Functional clustering of up-regulated proteins†	
Cluster	Enrichment score
Mitochondrial	6.86
Carbohydrate metabolic processes	5.78
Cytoskeleton	4.28
Mitochondrial lumen	4.20
FAD binding and reduction	3.70
Biotin/lipoyl attachment	3.02
Nucleoside binding	3.01
Catabolic processes	2.66
Longevity/aging	2.46
Muscle component	2.39
Catabolism and respiration	2.07
NAD binding and reduction	1.99
Cytoskeleton organization	1.39
Functional clustering of down-regulated proteins†	
Cluster	Enrichment score
Vitellogenins/reproduction	3.20
Mitochondrial	2.68
Galectins	2.07
Longevity/aging	1.59
Biosynthetic processes (DNA/RNA)	1.39

Functional analysis of the differential proteomics data. All enrichment analyses were performed using the Database for Annotation, Visualization and Integrated Discovery (DAVID) (23).

*Kyoto Encyclopedia of Genes and Genomes pathways overrepresented ($P < 0.05$) in the group of proteins up-regulated after metformin treatment.

†Functional clustering of proteins, which are significantly altered after metformin treatment. The reported enrichment score was calculated by DAVID according to the Fisher exact score of each clustered term. The higher the value, the more enriched the cluster. Only clusters with an enrichment score higher than 1 were reported. Complete information can be found in Dataset S1.

Metformin Does Not Induce Mitochondrial Protein Unfolding Stress. Because of the marked clustering of mitochondrial proteins (Table 1) and metformin's putative inhibitory effect on complex I of the ETC, it needs to be tested whether metformin is capable of inducing the mitochondria-specific unfolded protein response (UPR^{mt}). This is essential because the UPR^{mt} increases lifespan in response to either misfolding of mitochondrial proteins or stoichiometric abnormalities in the ETC complexes (24).

We did not observe up-regulation of the UPR^{mt} marker *hsp-6* in worms exposed to metformin (Fig. 1). Additional experiments with higher concentrations of metformin and different exposure times yielded similar negative results (Fig. S1). As such, lifespan extension of metformin via the induction of the UPR^{mt} is unlikely, which suggests that the drug affects the mitochondria in another way.

Metformin Increases Lifespan Through Hormetic Phenomena. Metformin has been put forward as a possible DR mimetic (7), and because DR has been linked to mitohormesis (13, 25), we looked into evidence for a role for mitohormesis in metformin-induced lifespan extension. Clustering analysis of the proteomics experiments revealed a significant overrepresentation of several mitochondrial proteins and proteins involved in catabolism (Table 1). These clusters might point to an increase in respiration, one of the hallmarks of mitohormesis (13). Indeed, upon metformin treatment, we observed a significant increase in respiration (45%) and metabolic heat production (38%) (Fig. 2*A*) in wild-type worms. These changes, in combination with the AMPK-dependence of metformin-mediated longevity (5), strongly resemble the mitohormetic pathway (13) and might point toward an increase in ROS production.

To verify whether mitochondrial ROS production was affected by metformin treatment, we measured hydrogen peroxide levels in metformin-treated worms. ROS production was indeed increased (Fig. 2*B*), further supporting the mitohormesis hypothesis. Induction of ROS production was already clear after 24 h of exposure to metformin (Fig. 2*B*). This increase in ROS seems to be an integral part of metformin-induced lifespan extension, because treatment with the potent antioxidants *N*-acetylcysteine (NAC) (13) and butylated hydroxyanisole (BHA) (26) abolished the positive effect of metformin on lifespan (Fig. 2*C* and

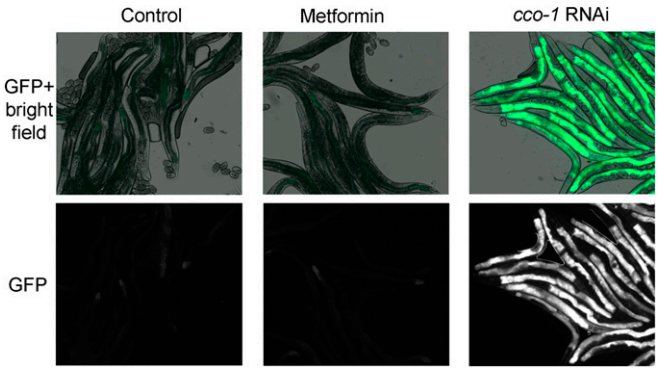

Fig. 1. Metformin treatment does not induce the mitochondria-specific unfolded protein response (UPR^{mt}). Day-1 adult metformin-treated *hsp-6*::GFP worms show no difference in fluorescence compared with untreated control worms. *hsp-6*::GFP worms were exposed to *cco-1* RNAi as a positive control. *cco-1* encodes a cytochrome *c* oxidase subunit, an integral part of the mitochondrial electron transport chain (24).

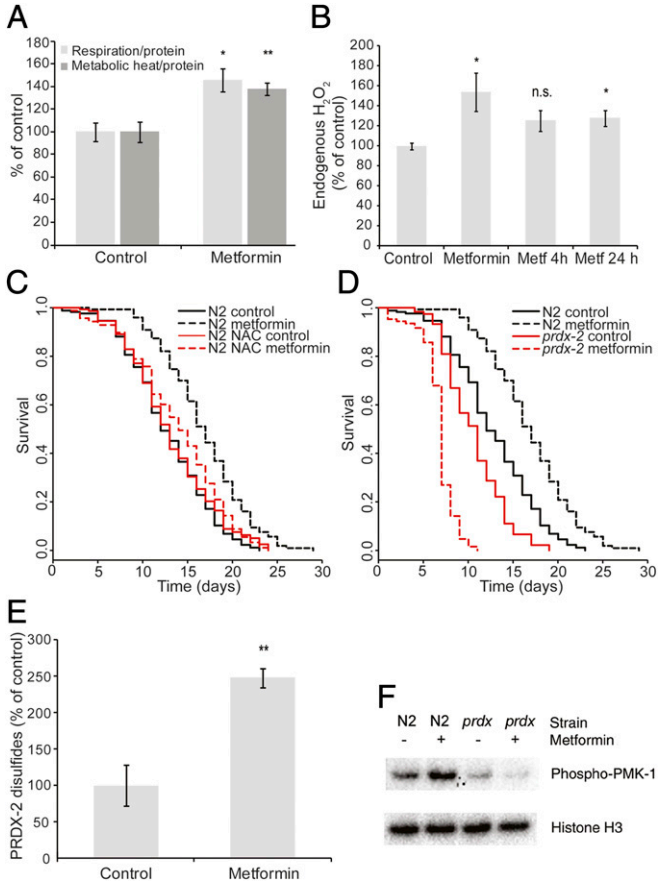

Fig. 2. Metformin increases lifespan according to the principle of mitohormesis, for which it requires PRDX-2. (*A*) Metformin treatment increases metabolic heat production (**$P < 0.01$; $n = 3$ for untreated and $n = 4$ for treated worms) and respiration (*$P < 0.05$; $n = 3$). Bars represent mean ± SEM. (*B*) Metformin induced a significant increase in H_2O_2 release in day-1 adult worms after both continuous exposure during development (*$P < 0.05$; $n = 7$) and after 24 h of exposure, starting from the young adult stage (*$P < 0.05$; $n = 7$ for untreated and $n = 5$ for treated worms). Exposing the worms for 4 h before measurement did not result in a significant increase ($^{n.s.}P > 0.05$; $n = 7$). Bars represent mean ± SEM. (*C*) The antioxidant NAC abolishes the lifespan-extending effect of metformin (***$P < 0.001$; $n \geq 169$ for each curve; Table S1). (*D*) *prdx-2* is required for metformin-induced lifespan extension. Metformin treatment significantly reduces lifespan of *prdx-2* mutants (***$P < 0.001$; $n \geq 127$ for each curve; Table S1). (*E*) Metformin treatment promotes the formation of PRDX-2 disulfide dimers (**$P < 0.01$), implied to function in signal transduction. Bars represent mean ± SEM ($n = 4$). (*F*) PRDX-2 is required for metformin-induced phosphorylation of the p38 MAP kinase PMK-1. Metformin treatment of wild-type worms induced phosphorylation of PMK-1, inferred from a larger band observed on the Western blot. This metformin-mediated induction of PMK-1 phosphorylation is absent in *prdx-2* knockout worms. Histone H3 levels were used as a loading control.

Fig. S2*A*). Finally, the critical phase for metformin-mediated lifespan extension clearly resembles the critical phase for other mitohormetic stressors (13), because treatment with metformin starting from adulthood onward or during the first few days of adulthood only were sufficient to increase lifespan. This is opposed to treatment with metformin during larval development only, which had no detectable effect on lifespan (Fig. S2*B*).

Metformin-Mediated Lifespan Extension Requires the Peroxiredoxin PRDX-2. The mitohormetic pathway as seen during glucose restriction is induced when low availability of glucose causes low energy levels, which in turn activates AMPK (13). AMPK activity increases catabolism and respiration, which results in the increased production of ROS and a resultant activation of hormetic protective mechanisms (13). The largest hiatus in this pathway is the step between the increased ROS production and the induction of stress defense: no molecule was put forward that might translate the ROS signal into further downstream defense. We therefore set out to reveal this missing link and to further complete the hormetic signaling pathway.

Peroxiredoxins are known hydrogen peroxide scavengers, and their oxidized dimeric form is involved in the direct activation of kinases in mammalian cells (27). Because the peroxiredoxin PRDX-2 was up-regulated during metformin treatment (Dataset S1), this protein is of particular interest as a potential inductor of mitohormesis. Deletion of the *prdx-2* gene results in an extreme decrease in lifespan upon metformin treatment (Fig. 2*D*). Not only did the positive effect of metformin on lifespan disappear, the *prdx-2* experimental group collapsed when exposed to metformin. Treatment with NAC partially rescued this deleterious effect, implying that excessive ROS production is at least partly responsible for the detrimental effect of metformin on these mutants (Fig. S2*C*). In support of these results, we observed increased formation of PRDX-2 dimers after metformin treatment (Fig. 2*E* and Fig. S3). Because these oxidized dimers are likely involved in cellular signaling (27), we propose that PRDX-2 induces prolongevity signaling during the mitohormetic response to metformin treatment.

One of the potential downstream targets of PRDX-2 is the p38 MAP kinase family-1 (PMK-1) protein, which is involved in the activation of the SKN-1 transcription factor (28). This transcription factor is in turn required for metformin-mediated longevity (5). Western blot analysis revealed a marked increase in phosphorylation of PMK-1 after metformin treatment. In contrast, deletion of *prdx-2* resulted in an absence of metformin-induced phosphorylation of PMK-1 (Fig. 2*F*). These data strongly imply that PRDX-2 is required for PMK-1 activation after metformin treatment.

In sum, all these findings subscribe that metformin extends lifespan via mitohormesis in *C. elegans* and that PRDX-2 is an integral part of the mitohormetic pathway.

Metformin Inhibits Complex I of the ETC. Metformin is generally believed to act through inhibition of complex I of the ETC (19–21), although some recent findings cast doubt on this (16, 22). Treatment of *C. elegans* with rotenone, another complex I inhibitor, at a concentration that extends longevity, results in a decrease in total oxygen consumption (25). Our finding that metformin increases respiration in worms therefore raises the question of whether it is truly capable of inhibiting complex I of the ETC.

We tested whether metformin is able to affect electron flow in mitochondria extracted from *C. elegans* and observed a clear and specific inhibition of electron flow from complex I, whereas the electron flow from complex II was unaffected (Fig. 3*A* and Fig. S4 *A* and *B*). These results, clearly mimicking the inhibitory action of rotenone (Fig. S4*A*), complement our previous data only if metformin inhibits complex I in a distinct way. To this end, we tested whether metformin and rotenone had different effects on ROS production in mitochondria. At concentrations at which both completely inhibit complex I respiration and after feeding only complex I, metformin increased ROS production, whereas rotenone decreased it (Fig. 3*B*), implying a fundamental difference between rotenone's and metformin's inhibitory action on complex I.

The BCAA Degradation Pathway Is Up-Regulated During Metformin Treatment. The BCAAs leucine, isoleucine, and valine display a certain duality in relation to health and longevity. On one hand

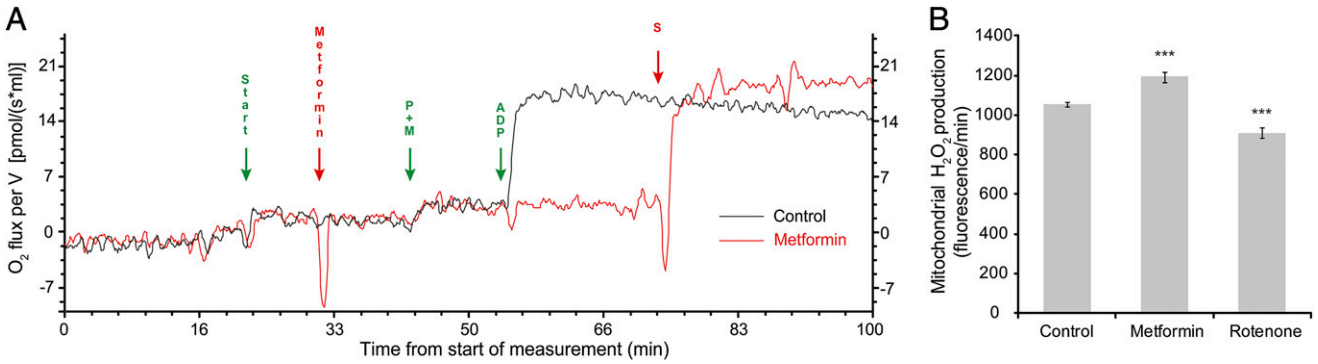

Fig. 3. Metformin inhibits complex I of the ETC in a way distinct from rotenone. (*A*) Metformin inhibits complex I- but not complex II-based respiration. Higher values for O_2 flux indicate higher respiration, negative values indicate a small influx of O_2, usually due to the injection of a compound. The effect of metformin on mitochondrial respiration was measured by sequentially adding compounds to stimulate different parts of the ETC. Green arrows indicate compounds that were added in both the control and metformin-treated cells; red arrows indicate compounds that were only added in the treated cell. After adding an equal volume of mitochondria (↓start), metformin was added to one of the cells (↓metformin). Subsequently, the complex I substrates pyruvate and malate (↓P+M) were added, followed by the addition of ADP (↓ADP), initiating electron transport from complex I. Metformin-treated mitochondria clearly fail to initiate complex I-based respiration, thus indicating that metformin inhibits electron transport from complex I in vitro. Finally, the complex II substrate succinate (↓S) was added to the metformin-treated cell, which led to a marked increase in mitochondrial respiration, indicating that metformin does not block electron transport from complex II. Two variations of this experiment were executed to also use the potent complex I inhibitor rotenone as a positive control (Fig. S4*A*) and to add succinate to the negative control condition as well (Fig. S4*B*). (*B*) Mitochondria treated with metformin produce H_2O_2 at a higher rate than untreated mitochondria (***$P < 0.001$; $n = 3$). Treatment with the complex I inhibitor rotenone had the opposite effect (***$P < 0.001$; $n = 3$).

their effectiveness has been noted in the treatment of liver and cardiac diseases (29, 30), and up-regulation of BCAAs is one of the metabolic signatures of the long-lived *daf-2* mutant (31, 32). On the other hand, BCAAs have also been causally linked to the development of insulin resistance, type II diabetes (33), and neuropathologies (34). We set out to confirm the marked up-regulation of the BCAA degradation pathway (Table 1 and Fig. S5) at the level of free BCAAs in metformin-treated worms. Metformin treatment resulted in a significant decrease (−55%) in the amount of free BCAAs, lending further support to the validity of the proteomics data (Fig. 4*A*).

Metabolic Flux During Metformin Treatment. One of the most striking properties of metformin as an antidiabetic in humans is its ability to cause weight loss in patients through, among others, activation of the β-oxidation pathway (2, 35, 36). We observed a 4.3-fold up-regulation of mitochondrial acyl-CoA dehydrogenase-1 (ACDH-1) after metformin treatment (Dataset S1), defining it as the strongest up-regulated protein by a margin. Acyl-CoA dehydrogenases catalyze the first step in the β-oxidation of fatty acids.

We questioned whether the shift in β-oxidation suggested by ACDH-1 induction truly occurs and whether it is involved in metformin-induced lifespan extension. If so, we would grossly expect overall fat levels to drop in treated worms. Measuring fat content in L4 worms, we found evidence for increased β-oxidation because metformin-treated worms showed significantly lower (−11.4%) fat stores (Fig. 4*B*). A similar reduction in fat content was found in metformin-treated *C. elegans* using different methods (5).

To our surprise, *acdh-1* knockout worms showed an even stronger metformin-induced lifespan extension than wild-type worms (Fig. 4*C*). This implies a more complex interaction between β-oxidation and metformin (*Discussion*).

Metformin-Treated Worms Attenuate Age-Related Morphological Decline. Aging worms start to show several morphological defects (37) and shrink in size (38), but metformin-treated worms seemed less affected by this phenomenon. After measuring several formalin-fixed worms of various ages (Fig. 5*A*) it became clear that nontreated worms started losing volume after day 6 of adulthood, whereas metformin-treated worms still

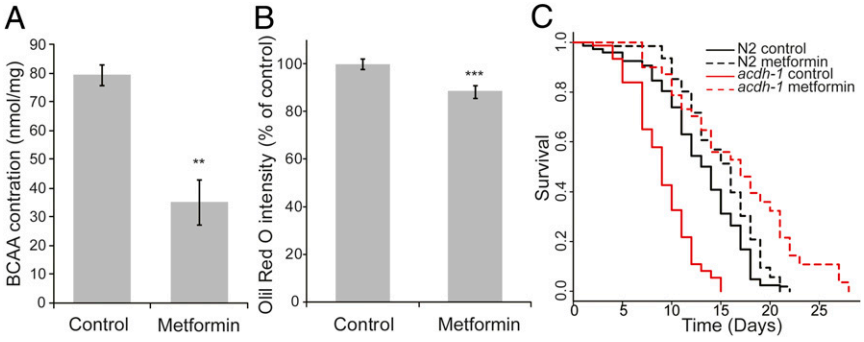

Fig. 4. Metformin induces the BCAA degradation and β-oxidation pathways but the β-oxidation enzyme ACDH-1 is not required for metformin-mediated longevity. (*A*) Metformin treatment stimulates the BCAA degradation pathway (Fig. S5) and in turn reduces the concentration of free BCAAs in *C. elegans* (**$P < 0.01$). Bars represent mean ± SEM ($n = 6$). (*B*) Metformin-treated worms show reduced fat storage (***$P < 0.001$; $n = 30$ for untreated and $n = 33$ for treated worms), possibly indicating increased flux through the β-oxidation pathway. Bars represent mean ± SEM. (*C*) Deletion of β-oxidation enzyme *acdh-1* results in a proportionally larger effect of metformin on longevity (***$P < 0.001$; $n \geq 54$ for each curve; Table S1).

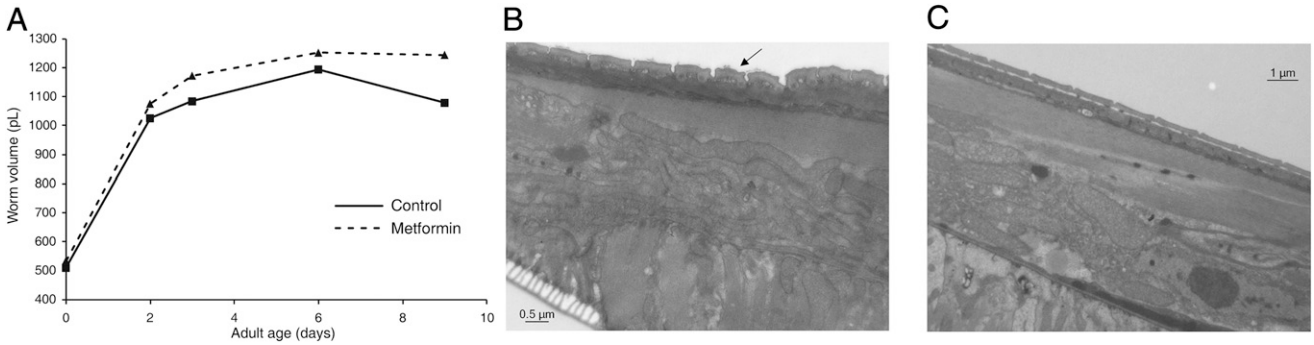

Fig. 5. Metformin attenuates the morphological decline with aging in *C. elegans*. (*A*) Metformin-treated worms retain a stable volume, whereas control worms older than 6 d start shrinking. (*B*) Electron micrograph of the cuticle of a day-9 adult nontreated wild-type worm. Some deformations of the cuticle (seen as "wrinkling," marked with an arrow) are starting to manifest. (*C*) No structural abnormalities can be seen in a metformin-treated day-9 wild-type adult.

retained their normal volume on day 9. Although long-lived mutants are often smaller than their wild-type siblings (39), our results fit the recent observations that within isogenic populations the larger animals are generally the longer-lived ones (38).

Muscle and cuticle are known to show severe morphological defects with increasing age in *C. elegans* (37), making them prime targets to question whether these tissues are better maintained in metformin-treated worms. Our proteomics data already pointed to an increase in muscle mass and several changes in the cytoskeleton (Table 1), including up-regulation of intermediate filament proteins (Dataset S1). Electron micrographs of 9-d-old control and metformin-treated worms displayed no difference in body wall muscle volume, but there was a clear difference in cuticle morphology (Fig. 5 *B* and *C*). Whereas the cuticle of 9-d-old adult nontreated worms started showing signs of age-related "wrinkling" and disorganization, the cuticle of metformin-treated worms resembled that of a young animal. Considering the cuticle's known role in maintaining the shape and size of nematodes (40), it can be assumed that it is this amelioration of cuticle deterioration that allows metformin-treated worms to retain a healthy, young morphology.

Discussion

We profiled the effect of metformin in *C. elegans* using a differential proteomics approach and used the resulting data for further examination of its beneficial effects and mode of action.

We observed many changes in the mitochondrial proteome, which might point toward mitonuclear protein imbalance (41) and an altered mitochondrial metabolism. It is therefore probable for metformin to increase lifespan through both the process of mitohormesis and the induction of the UPR^{mt}. However, metformin administration during the larval stages had no effect on lifespan, whereas the critical phase for UPR^{mt} induction in *C. elegans* is during larval development (24, 42). Because metformin also proved unable to induce the UPR^{mt}, it is not a likely in vivo contributor to lifespan extension by metformin in *C. elegans*. Contrary to the UPR^{mt}, the mitohormetic pathway is important for metformin-mediated longevity in this worm.

Hormesis in aging is defined as the process by which a short-term and nonlethal stressor induces the stress response mechanisms of an organism and thereby increases stress resistance and overall life expectancy (43). The mitohormetic pathway, first described in glucose-restricted *C. elegans* (13), states that a low availability of ATP—due to low glycolytic activity—causes activation of AMPK. AMPK in turn promotes general catabolism and mitochondrial respiration, leading to increased production of ROS (the hormetic "stressor"), which subsequently act as messengers to activate further stress defenses, prolonging lifespan. This contradicts the classic oxidative stress theory of aging, which postulates that ROS, because of their ability to damage biomolecules, would be the causative factor of aging (44). We were able to fully reproduce the mitohormetic phenomenon in metformin-treated worms and showed that metformin increases respiration, metabolic heat production, and ROS generation in *C. elegans*. Inhibition of ROS signaling abolishes the lifespan-extending effects of metformin, proving that metformin-mediated lifespan extension is dependent on the mitohormetic pathway and most closely resembles the *C. elegans* response to glucose restriction.

Although well studied, some major missing links remained in the mitohormetic pathway, in particular how the ROS signal can be translated to increased lifespan. We were able to demonstrate that the *C. elegans* peroxiredoxin PRDX-2, previously shown to be involved in peroxide and heavy metal resistance (45), is of major importance to this function. Peroxiredoxins are a class of antioxidant proteins characterized by their high susceptibility to cysteine oxidation (46, 47). PRDX-2 is a typical 2-Cys peroxiredoxin (45), of which the active, oxidized form exists as a homodimer (48). It has recently been shown that these dimers are subsequently able to oxidize and activate specific substrates, such as the MAP kinase ASK1 (27), thus resolving how these proteins might be able to translate ROS signals into downstream signaling. In the same vein, our experiments revealed increased formation of PRDX-2 dimers after metformin treatment. These oxidized dimers might activate ASK1's closest ortholog in *C. elegans,* the MAP kinase NSY-1, which functions upstream in the same signaling pathway as the MAP kinases SEK-1 and PMK-1 (49). This evolutionarily conserved MAP kinase cascade could ultimately activate several downstream targets that mediate stress defense, including SKN-1 (28). We showed that *prdx-2* is required for the downstream activation of PMK-1 in response to metformin exposure, completing the pathway (Fig. 6). Therefore, PRDX-2 may well be the protein responsible for translating oxidative stress into longer lifespan in *C. elegans*. Because the longevity-promoting effect of exercise in humans also depends on ROS signaling (50), this pathway may be evolutionarily conserved.

AMPK activation is one of the main factors involved in mitohormetic lifespan extension (13, 26). Although metformin is known to activate AMPK, exactly how this occurs remains elusive. The most common hypothesis is that metformin is able to partially inhibit complex I of the mitochondrial ETC, which in turn would lead to energy depletion and activation of AMPK (19–21). Recently this has been debated (16, 22). One of the main arguments against metformin-mediated inhibition of complex I is the increased activity of pathways that generate energy after metformin treatment. All these pathways require NAD^+ to function, and without efficient recycling of NADH to NAD^+,

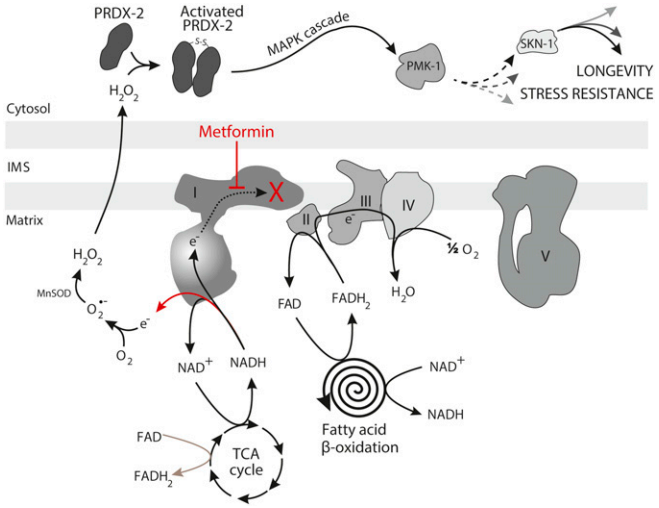

Fig. 6. The mitohormetic signaling cascade as induced by metformin. Metformin induces an increase in activity in several catabolic pathways (Fig. S6), including the TCA cycle and β-oxidation, with β-oxidation producing a relatively higher amount of $FADH_2$ per cycle. This increase in substrate allows for an increase in mitochondrial respiration, which in turn leads to an increase in ROS production, possibly through metformin-mediated perturbation of electron transport (marked in red). These ROS oxidize PRDX-2 peroxiredoxins, which subsequently dimerize and enter their active state. Active PRDX-2 will activate a conserved MAPK cascade containing the p38 MAPK PMK-1, likely leading to the activation of SKN-1 (28) and a concomitant increase in longevity and stress protection (dashed arrows: literature-based evidence; Fig. S6 provides more information on the pathways induced by metformin treatment).

these pathways are limited in activity. Because NADH is mainly recycled at complex I of the ETC, blocking complex I should lead to an increased NADH/NAD^+ ratio and lower catabolism (Fig. 6). As a case in point, the complex I inhibitor rotenone indeed increases the NADH/NAD^+ ratio (51) and lowers the activity of the β-oxidation pathway (16). We were able to show that metformin specifically inhibits complex I of the ETC in vitro, albeit in a way that seems fundamentally distinct from rotenone: metformin increased mitochondrial ROS production, whereas rotenone decreased it. High concentrations of rotenone reduce the number of electrons that are transferred from NADH to complex I (high NADH/NAD^+ ratio), hence less electrons can leak out to form ROS. Our results imply that upon metformin treatment, NADH is still able to transfer its electrons, but these are subsequently lost, resulting in increased ROS production (Fig. 6). On the basis of these data, we suggest that metformin activates AMPK through inhibition of complex I (Fig. S6), which leads to an increase in respiration and a concomitant up-regulation of several catabolic pathways (e.g., β-oxidation, glycolysis, BCAA catabolism, and others) to provide the necessary substrate for the ETC. Likely exacerbated by metformin-mediated perturbation of electron transport, the increase in respiration ultimately leads to a mitohormetic increase in ROS production in vivo (Fig. 6). Because elevated respiration under physiologically normal conditions often leads to a reduction in ROS production (31), this indeed implies a direct involvement of metformin in the observed increase in ROS.

Treatment of *C. elegans* with metformin results in an overall up-regulation of several pathways and processes (including glycolysis and the TCA cycle), most of which are involved in catabolism, supporting the shift toward increased respiration. Two catabolic pathways stood out after metformin treatment: β-oxidation, through the short chain acyl-CoA dehydrogenase ACDH-1, and BCAA degradation. In light of metformin's inhibitory action on complex I but not complex II of the ETC, the observed increase in β-oxidation seems a logical adaptation because it produces a relatively high amount of the complex II substrate $FADH_2$ compared with other catabolic pathways. This might explain why knocking out *acdh-1* adds to the lifespan increase induced by metformin: high activity of the β-oxidation pathway could temporarily increase ATP levels and inactivate AMPK (Fig. 6 and Fig. S6). As such, deletion of *acdh-1* could cause a more stringent activation of the mitohormetic pathway. Further experiments will be needed to fully explore the role of β-oxidation in metformin-induced lifespan extension. Our results suggest that the metformin-mediated increase in β-oxidation is likely a compensatory mechanism that is unrelated to metformin-induced longevity.

As for the BCAA degradation pathway, no clear singular correlation between BCAAs and longevity has yet been found in any organism. Although some evidence points toward BCAAs as a metabolic signature of long life in *C. elegans* insulin receptor mutants (31, 32), other studies have causally linked BCAAs to the development of insulin resistance, diabetes (33), and neuropathologies (34). Interestingly, BCAAs, leucine in particular, are potent activators of the target of rapamycin (TOR) kinase. Leucine deprivation has previously been associated with reduced TOR signaling (52), which can in turn prolong lifespan and is required for DR-mediated lifespan extension (53). However, it remains unclear whether the drop in BCAA levels is necessary for metformin-induced lifespan extension. The reduction in BCAA concentration might result in lower RNA translation into protein, both through inactivation of TOR and a reduction in the amount of substrate necessary for translation (Fig. S6). This in turn may lead to an increase in longevity. There is some precedence for this hypothesis: amino acid imbalance has been associated with increased longevity in *Drosophila melanogaster* (54), among others (55). The recently described bacteria-specific effect of metformin on longevity in *C. elegans* (6) might similarly depend on an amino acid imbalance that occurs through the lowered production of methionine in metformin-treated bacteria (Fig. S6). Our results suggest a hitherto unexplored role for the BCAA degradation pathway in longevity.

Metformin not only increases lifespan but also healthspan of *C. elegans*: treated worms retain a youthful morphology for a longer time. How metformin is able to attenuate morphological decline of the cuticle in *C. elegans* remains elusive, but the intermediate filament protein IFC-2 (up-regulated after metformin treatment; Dataset S1) seems particularly promising because it is required for normal body shape and cuticle strength (56). Integrity of the cuticle and epidermis might play a more important role in longevity than is generally thought. Deterioration in cuticle structure leads to a loss in barrier function, which may be one of the causes of death of older nematodes (37, 40).

In conclusion, this work reveals insights in the process of aging and shows that metformin extends lifespan through mitohormesis. A missing link in the mitohormesis pathway in *C. elegans* has now been assigned: the peroxiredoxin PRDX-2, a protein that translates a ROS signal into a prolongevity cue. Because peroxiredoxin signaling is evolutionarily conserved (27), peroxiredoxins might hold a similar function in humans.

Materials and Methods

***C. elegans* Strains.** The following strains were obtained from the *Caenorhabditis* Genetics Center (University of Minnesota): wild-type N2, VC289 *prdx-2(gk169)*, VC1011 *acdh-1(ok1489)*, and SJ4100 *zcIs13[hsp-6::GFP]*. GA507 *glp-4(bn2ts) daf-16(mgDf50)* was provided by the Gems laboratory. Strains were cultivated on standard nematode growth medium (NGM) seeded with *Escherichia coli* OP50. All strains were outcrossed at least four times, with the exception of SJ4100, which was outcrossed three times. The outcrossed *prdx-2(gk169)* and *acdh-1(ok1489)* strains were renamed LSC555 and LSC556, respectively. All experiments were performed at 20 °C unless stated otherwise.

Sampling for Two-Dimensional Difference Gel Electrophoresis. The protein samples for two-dimensional difference gel electrophoresis (2D-DIGE) were taken from *glp-4(bn2ts) daf-16(mgDf50)* worms grown in liquid cultures. The *glp-4(bn2ts)* mutation confers sterility at the permissive temperature of 24 °C, avoiding contamination with progeny. Preventing germ-line development also removes abundant contaminating proteins that have no bearing on lifespan, facilitating the analyses. Because *glp-4* mutations cause a slight DAF-16–dependent lifespan increase in *C. elegans* cultured on dead *E. coli* (57), *glp-4(bn2ts) daf-16(mgDf50)* double mutants were used. This does not interfere with the envisaged results, because lifespan extension due to metformin is independent of DAF-16 (5). Cultivating the worms in liquid cultures allowed full control over metformin dosage while ensuring that all worms were fully fed. Additionally, the high-density samples obtained from liquid cultures ensure high protein concentration in 2D-DIGE experiments.

Worms were synchronized by isolating eggs from gravid adults through hypochlorite and NaOH treatments (58) and a subsequent sucrose density centrifugation to separate eggs from dead worms and bacterial debris. L1 worms were added to Fernbach flasks containing S medium (59) and constantly shaken at 24 °C. Flash frozen *E. coli* K12 bacteria (Artechno) were added to the cultures as food source. The concentration of bacteria was checked twice daily, and new K12 bacteria were added accordingly to maintain the cultures at optimal food levels (OD_{550} = 1.8). The density of worms in the culture never exceeded 1,000 worms/mL to prevent large fluctuations in food availability. When worms reached the L4 stage, cultures were supplemented with 2′-deoxy-5-fluorouridine (FUdR; Sigma-Aldrich) at a final concentration of 100 mg/L. This ensures complete sterility, because *glp-4(bn2ts) daf-16(mgDf50)* worms rarely manage to produce a few eggs. Once worms reached the adult stage, the test group was exposed to 25 mM of metformin (1,1-dimethylbiguanide hydrochloride; Sigma-Aldrich) for 24 h (*SI Materials and Methods* describes the determination of the optimal metformin concentration in liquid media; Fig. S7), and protein samples were subsequently taken (*SI Materials and Methods* provides a complete protocol on protein extraction).

2D-DIGE. Samples were labeled, separated, and analyzed as described by Bogaerts et al. (60). In short, metformin-treated and nontreated protein extracts were differentially labeled with either Cy3 or Cy5 fluorescent dyes (GE Healthcare). A possible dye bias was taken into account by integrating a dye swap into the experimental design. Differentially labeled samples were pooled, an internal standard labeled with Cy2 was added, and the pooled samples were separated in two dimensions. Gels were scanned using an Ettan DIGE Imager (GE Healthcare), and DeCyder 7.0 (GE Healthcare) was used to statistically analyze the images. Spot intensity was compared using a standard Student *t* test with false positive rate correction.

Trypsin Digestion and Identification of Differential Proteins. Differential spots were excised using an automated spotpicker (GE Healthcare). The proteins in each spot were digested using a standard in-gel trypsin digestion protocol and subsequently identified using peptide mass fingerprinting (*SI Materials and Methods* provides a complete protocol).

Clustering of Differential Proteins. Wormbase gene IDs of differential proteins were uploaded to the bioinformatic tool DAVID (23) to look for enrichment in functional clusters. Functional clustering was performed with high stringency. Pathway enrichment was determined using DAVID by querying the Kyoto Encyclopedia of Genes and Genomes.

Lifespan Experiments. All lifespan experiments were performed on NGM agar plates or NGM plates supplemented with or without 50 mM of metformin. NAC was used at a concentration of 5 mM and BHA at a concentration of 25 μM, when applicable. For the experiment using BHA, the compound was added from a 1,000× concentrated stock in DMSO, and an equal volume of DMSO was added to the respective controls. The worms used in the BHA lifespan experiment were pretreated with 25 μM of BHA for one generation before the start of the experiment. For lifespan experiments, 20 L4 stage worms from a synchronous culture were transferred to a plate (either regular NGM or NGM containing one or multiple of the tested compounds), allowed to lay eggs for 24 h, and were then removed from the plate. The progeny was transferred to a new plate when they reached the young adult stage and were transferred to new plates during each day of their reproductive period and every 3 d thereafter. Lifespan was monitored every day starting from day 1 of the adult stage: animals that did not move when gently prodded were marked as dead. Animals that crawled off the plate or died of vulval bursting or internal hatching were censored. Survival curves were statistically analyzed using a Cox proportional hazard (to compare the effect of metformin between strains and/or conditions) or log–rank test (to compare a single curve to control; corrected for multiple testing using the Benjamini-Hochberg method). Complete information regarding lifespan experiments can be found in the SI (Table S1).

Measuring *hsp-6*::GFP Fluorescence. Synchronized L1 worms of the SJ4100 *zcIs13[hsp-6::GFP]* strain were transferred to agar plates containing 0 mM, 50 mM, or 100 mM of added metformin. As a positive control, worms were transferred to plates seeded with HT115 *Escherichia coli* containing an RNAi construct targeted against *cco-1* (24). To rule out a specific effect of HT115, plates seeded with HT115 containing an empty vector were used, which caused no fluorescence. Images were acquired using a Zeiss Axio Imager Z1 microscope.

Measuring Metabolic Heat and Respiration. Metabolic activity and respiration measurements were carried out as previously described (61). In short, respiration and metabolic heat production of synchronized day-1 adult worms were measured using a Clark-type electrode respirometer (Strathkelvin) and a Thermal Activity Monitor (Thermometric), respectively. Treated worms were exposed to 50 mM metformin starting from the L1 stage. Oxygen consumption rates were measured over a span of 15 min. After thermal equilibration of the calorimeter, live heat output of each sample was averaged over a 3-h period. All data were normalized according to the protein concentration in each sample, because this directly correlates to worm biomass. Protein concentrations were determined using a bicinchoninic acid kit (Thermo Scientific). Student *t* tests were used to statistically analyze the data.

Quantifying in Vivo Hydrogen Peroxide Production. Endogenous hydrogen peroxide production was quantified using the Amplex Red hydrogen peroxide kit (Invitrogen, catalog no. A22188). Adult worms were washed three times with S basal (59), after which the worms were pelleted through centrifugation (800 × *g*, 3 min). From this dense pellet, 50 μL of worms were transferred to a new microcentrifuge tube containing 450 μL of reaction buffer (sodium phosphate buffer supplied with the kit). After centrifugation (800 × *g*, 1.5 min), the reaction buffer was replaced with fresh reaction buffer, and 500 μL of Amplex Red working solution (prepared according to the manufacturer's instructions) was added. The worms were allowed to rotate in the dark for 1 h, after which they were pelleted through centrifugation (800 × *g*, 1.5 min), and 100 μL of supernatant was transferred to a fluorescence-compatible 96-well plate. Fluorescence (Ex 550 nm, Em 590 nm) was measured, and the worm pellet was subjected to protein extraction for normalization. Welch's *t* tests with multiple testing correction (Benjamini-Hochberg) were used to statistically analyze the heteroscedastic data.

Measuring Mitochondrial Respiration. Mitochondria were extracted from worms as previously described (62). Oxygen consumption of the extracted mitochondria was determined using a Clark-type electrode (Oxygraph 2k) and DatLab software (Oroboros Instruments). An aliquot of 25 μL of mitochondria was incubated in 2 mL of air-saturated MiR05 (0.5 mM EGTA, 3 mM $MgCl_2$, 60 mM K-lactobionate, 20 mM taurine, 10 mM KH_2PO_4, 20 mM Hepes, 110 mM sucrose, and 1 g/L BSA, pH 7.1) at 20 °C. The effect of 25 mM of metformin on electron transport from complex I and complex II was measured as follows: (*i*) metformin was added from a 1.5-M stock (dissolved in MiR05) until a final concentration of 25 mM was reached; (*ii*) the complex I substrates pyruvate and malate were added from a 1-M stock until a final concentration of 5 mM was reached; (*iii*) ADP was added from a 10-mM stock to initiate complex I respiration (final concentration 25 μM); (*iv*) when applicable, rotenone was added as a positive control at a final concentration of 1 μg/mL from a 400-μg/mL stock; (*v*) to initiate complex II respiration, succinate was added from a 1-M stock until a final concentration of 5 mM was reached.

Measuring Mitochondrial Hydrogen Peroxide Production. Mitochondrial hydrogen peroxide production was quantified using a protocol based on the Amplex Red hydrogen peroxide kit (Invitrogen, catalog no. A22188). A fluorescence-compatible 96-well plate was prepared, and several wells were filled with 96 μL of incubation medium (4 mM ADP, 10 mM pyruvate, 10 mM malate, 10 U Cu/ZnSOD) either containing no additional substance, 25 mM of metformin, or 1 μg/mL of rotenone. Subsequently, 100 μL of Amplex Red reaction buffer (100 μM Amplex Red, 4 U/mL horseradish peroxidase dissolved in the sodium phosphate buffer supplied with the kit) was added, followed by the addition of 4 μL of freshly extracted mitochondria. The plate was shaken in the dark, and every 2 min fluorescence (Ex 550 nm, Em 590 nm) was measured over the span of 1 h to accurately plot the increase in fluorescence

over time resulting from hydrogen peroxide production. The resulting curves were statistically analyzed using analysis of covariance.

Anti-PRDX-2 Western Blot. A nonreducing anti-PRDX-2 Western blot was performed as described by Oláhová et al. (45). In short, synchronized L1 worms were grown on NGM plates with or without 50 mM of added metformin. Proteins were extracted from young adult worms and separated on a nonreducing SDS/PAGE gel. Rabbit anti-PRDX-2 antibodies were kindly provided by Elizabeth Veal (Newcastle University, Newcastle upon Tyne, UK). Intensity of PRDX-2 bands was normalized against total protein content of each lane, which was visualized using a Deep Purple (GE Healthcare) total protein stain. A Welch's *t* test was performed to analyze the data.

Anti Phospho-PMK-1 Western Blot. N2 and *prdx-2* worms were synchronized and grown on regular NGM plates. Protein samples of day-1 adult worms were taken as described for the 2D-DIGE experiment. Proteins were separated on an SDS/PAGE gel, and rabbit anti-phospho-p38 antibodies were used for visualization (Cell Signaling Technology). Blots were reincubated with rabbit anti-histone H3 antibodies (Abcam) as a loading control (63).

Measuring Fat Content Through Oil Red O Staining. Synchronized L1 worms were cultivated on NGM plates with or without 50 mM of added metformin. L4 stage worms were harvested and stained with Oil red O. The staining intensity was acquired for at least 30 worms for each condition (*SI Materials and Methods*). A Student *t* test was performed to analyze the data.

Measuring Worm Volume. Wild-type worms were synchronized through hypochlorite treatment, and L1 worms were transferred to normal NGM plates or NGM plates supplemented with 50 mM of metformin. FUdR was added to the plates when worms reached the L4 stage at a final concentration of 50 μM. For sampling, worms were washed twice with S basal and subsequently fixed in 4% (wt/vol) formaldehyde (3 min at 65 °C). Images of the formaldehyde fixed worms were captured, and worm width (D) and length (L) were analyzed using a RapidVUE Particle Shape and Size Analyzer (Beckman Coulter). Worm volume was approximated using the cylinder formula $[V = \pi L(D/2)^2]$.

Electron Micrographs. Wild-type worms were synchronized and sterilized as described for the volume measurements. Worms were harvested when they reached day 9 of adulthood and prepared for electron microscopy (*SI Materials and Methods*).

Quantifying Concentration of BCAAs. Wild-type worms were synchronized, and L4 worms were harvested from the plates. BCAA concentration was measured using a BCAA assay kit (Sigma-Aldrich, catalog no. MAK003) according to manufacturer's instructions. Total protein content of the extracts was quantified using the Qubit Protein Assay (Invitrogen) and used for normalization. A Welch's *t* test was performed to analyze the data.

Statistical Analysis. All statistical analyses, apart from the DeCyder and DAVID analysis, were carried out using R (64). All bar graphs show the mean of biologically independent samples, and error bars show SEM. *P* values <0.05 were considered significant.

ACKNOWLEDGMENTS. We thank Dr. Elizabeth Veal for providing the anti-PRDX-2 antibodies; Prof. Dr. David Gems for providing the GA507 strain; and Sven Van Bael, An Vandoren, Caroline Vlaeminck, and Ineke Dhondt for technical assistance. Several strains were provided by the *Caenorhabditis* Genetics Center, which is funded by National Institutes of Health Office of Research Infrastructure Programs Grant P40 OD010440. This work was supported by a grant from the Fund for Scientific Research–Flanders (Fonds voor Wetenschappelijk Onderzoek Vlaanderen; FWO-Flanders) (G.04371.0N). L.T. is an FWO-Flanders postdoctoral fellow.

1. Anisimov VN, et al. (2008) Metformin slows down aging and extends life span of female SHR mice. *Cell Cycle* 7(17):2769–2773.
2. Martin-Montalvo A, et al. (2013) Metformin improves healthspan and lifespan in mice. *Nat Commun* 4:2192.
3. Rizos CV, Elisaf MS (2013) Metformin and cancer. *Eur J Pharmacol* 705(1-3):96–108.
4. Nakajima K (2012) Multidisciplinary pharmacotherapeutic options for nonalcoholic fatty liver disease. *Int J Hepatol* 2012:950693.
5. Onken B, Driscoll M (2010) Metformin induces a dietary restriction-like state and the oxidative stress response to extend *C. elegans* Healthspan via AMPK, LKB1, and SKN-1. *PLoS ONE* 5(1):e8758.
6. Cabreiro F, et al. (2013) Metformin retards aging in *C. elegans* by altering microbial folate and methionine metabolism. *Cell* 153(1):228–239.
7. Ingram DK, et al. (2006) Calorie restriction mimetics: An emerging research field. *Aging Cell* 5(2):97–108.
8. Fontana L, Partridge L, Longo VD (2010) Extending healthy life span—from yeast to humans. *Science* 328(5976):321–326.
9. Dhahbi JM, Mote PL, Fahy GM, Spindler SR (2005) Identification of potential caloric restriction mimetics by microarray profiling. *Physiol Genomics* 23(3):343–350.
10. Bishop NA, Guarente L (2007) Two neurons mediate diet-restriction-induced longevity in *C. elegans*. *Nature* 447(7144):545–549.
11. Panowski SH, Wolff S, Aguilaniu H, Durieux J, Dillin A (2007) PHA-4/Foxa mediates diet-restriction-induced longevity of *C. elegans*. *Nature* 447(7144):550–555.
12. Greer EL, Brunet A (2009) Different dietary restriction regimens extend lifespan by both independent and overlapping genetic pathways in *C. elegans*. *Aging Cell* 8(2):113–127.
13. Schulz TJ, et al. (2007) Glucose restriction extends *Caenorhabditis elegans* life span by inducing mitochondrial respiration and increasing oxidative stress. *Cell Metab* 6(4):280–293.
14. Zhou G, et al. (2001) Role of AMP-activated protein kinase in mechanism of metformin action. *J Clin Invest* 108(8):1167–1174.
15. Stephenne X, et al. (2011) Metformin activates AMP-activated protein kinase in primary human hepatocytes by decreasing cellular energy status. *Diabetologia* 54(12):3101–3110.
16. Ouyang J, Parakhia RA, Ochs RS (2011) Metformin activates AMP kinase through inhibition of AMP deaminase. *J Biol Chem* 286(1):1–11.
17. Foretz M, et al. (2010) Metformin inhibits hepatic gluconeogenesis in mice independently of the LKB1 / AMPK pathway via a decrease in hepatic energy state. *J Clin Invest* 120:2355–2369.
18. Ben Sahra I, et al. (2011) Metformin, independent of AMPK, induces mTOR inhibition and cell-cycle arrest through REDD1. *Cancer Res* 71(13):4366–4372.
19. Owen MR, Doran E, Halestrap AP (2000) Evidence that metformin exerts its anti-diabetic effects through inhibition of complex 1 of the mitochondrial respiratory chain. *Biochem J* 348(Pt 3):607–614.
20. El-Mir MY, et al. (2000) Dimethylbiguanide inhibits cell respiration via an indirect effect targeted on the respiratory chain complex I. *J Biol Chem* 275(1):223–228.
21. Ota S, et al. (2009) Metformin suppresses glucose-6-phosphatase expression by a complex I inhibition and AMPK activation-independent mechanism. *Biochem Biophys Res Commun* 388(2):311–316.
22. Larsen S, et al. (2012) Metformin-treated patients with type 2 diabetes have normal mitochondrial complex I respiration. *Diabetologia* 55(2):443–449.
23. Huang W, et al. (2007) The DAVID Gene Functional Classification Tool: A novel biological module-centric algorithm to functionally analyze large gene lists. *Genome Biol* 8(9):R183.
24. Durieux J, Wolff S, Dillin A (2011) The cell-non-autonomous nature of electron transport chain-mediated longevity. *Cell* 144(1):79–91.
25. Schmeisser S, et al. (2013) Neuronal ROS signaling rather than AMPK/sirtuin-mediated energy sensing links dietary restriction to lifespan extension. *Mol Metab* 2(2):92–102.
26. Zarse K, et al. (2012) Impaired insulin/IGF1 signaling extends life span by promoting mitochondrial L-proline catabolism to induce a transient ROS signal. *Cell Metab* 15(4):451–465.
27. Jarvis RM, Hughes SM, Ledgerwood EC (2012) Peroxiredoxin 1 functions as a signal peroxidase to receive, transduce, and transmit peroxide signals in mammalian cells. *Free Radic Biol Med* 53(7):1522–1530.
28. Inoue H, et al. (2005) The *C. elegans* p38 MAPK pathway regulates nuclear localization of the transcription factor SKN-1 in oxidative stress response. *Genes Dev* 19(19):2278–2283.
29. Lam VW, Poon RT (2008) Role of branched-chain amino acids in management of cirrhosis and hepatocellular carcinoma. *Hepatol Res* 38(Suppl 1):S107–S115.
30. Mitręga K, et al. (2011) Beneficial effects of l-leucine and l-valine on arrhythmias, hemodynamics and myocardial morphology in rats. *Pharmacol Res* 64(3):218–225.
31. Fuchs S, et al. (2010) A metabolic signature of long life in *Caenorhabditis elegans*. *BMC Biol* 8:14.
32. Depuydt G, et al. (2013) Reduced insulin/insulin-like growth factor-1 signaling and dietary restriction inhibit translation but preserve muscle mass in *Caenorhabditis elegans*. *Mol Cell Proteomics* 12(12):3624–3639.
33. Newgard CB (2012) Interplay between lipids and branched-chain amino acids in development of insulin resistance. *Cell Metab* 15(5):606–614.
34. De Simone R, et al. (2013) Branched-chain amino acids influence the immune properties of microglial cells and their responsiveness to pro-inflammatory signals. *Biochim Biophys Acta* 1832(5):650–659.
35. Stachowicz A, et al. (2012) Proteomic analysis of liver mitochondria of apolipoprotein E knockout mice treated with metformin. *J Proteomics* 77:167–175.
36. Lee A, Morley JE (1998) Metformin decreases food consumption and induces weight loss in subjects with obesity with type II non-insulin-dependent diabetes. *Obes Res* 6(1):47–53.
37. Herndon LA, et al. (2002) Stochastic and genetic factors influence tissue-specific decline in ageing *C. elegans*. *Nature* 419(6909):808–814.
38. Pincus Z, Smith-Vikos T, Slack FJ (2011) MicroRNA predictors of longevity in *Caenorhabditis elegans*. *PLoS Genet* 7(9):e1002306.

39. Iser WB, Wolkow CA (2007) DAF-2/insulin-like signaling in *C. elegans* modifies effects of dietary restriction and nutrient stress on aging, stress and growth. *PLoS ONE* 2(11): e1240.
40. Chisholm AD, Xu S (2012) The *Caenorhabditis elegans* epidermis as a model skin. II: Differentiation and physiological roles. *Wiley Interdiscip Rev Dev Biol* 1(6):879–902.
41. Houtkooper RH, et al. (2013) Mitonuclear protein imbalance as a conserved longevity mechanism. *Nature* 497(7450):451–457.
42. Dillin A, et al. (2002) Rates of behavior and aging specified by mitochondrial function during development. *Science* 298(5602):2398–2401.
43. Rattan SIS (2008) Hormesis in aging. *Ageing Res Rev* 7(1):63–78.
44. Harman D (1956) Aging: A theory based on free radical and radiation chemistry. *J Gerontol* 11(3):298–300.
45. Oláhová M, et al. (2008) A redox-sensitive peroxiredoxin that is important for longevity has tissue- and stress-specific roles in stress resistance. *Proc Natl Acad Sci USA* 105(50):19839–19844.
46. Yang K-S, et al. (2002) Inactivation of human peroxiredoxin I during catalysis as the result of the oxidation of the catalytic site cysteine to cysteine-sulfinic acid. *J Biol Chem* 277(41):38029–38036.
47. Thamsen M, Kumsta C, Li F, Jakob U (2011) Is overoxidation of peroxiredoxin physiologically significant? *Antioxid Redox Signal* 14(4):725–730.
48. Hall A, Karplus PA, Poole LB (2009) Typical 2-Cys peroxiredoxins—structures, mechanisms and functions. *FEBS J* 276(9):2469–2477.
49. Kim DH, et al. (2002) A conserved p38 MAP kinase pathway in *Caenorhabditis elegans* innate immunity. *Science* 297(5581):623–626.
50. Ristow M, et al. (2009) Antioxidants prevent health-promoting effects of physical exercise in humans. *Proc Natl Acad Sci USA* 106(21):8665–8670.
51. He Q, Wang M, Petucci C, Gardell SJ, Han X (2013) Rotenone induces reductive stress and triacylglycerol deposition in C2C12 cells. *Int J Biochem Cell Biol* 45(12):2749–2755.
52. Xiao F, et al. (2011) Leucine deprivation increases hepatic insulin sensitivity via GCN2/mTOR/S6K1 and AMPK pathways. *Diabetes* 60(3):746–756.
53. Hansen M, et al. (2007) Lifespan extension by conditions that inhibit translation in *Caenorhabditis elegans*. *Aging Cell* 6(1):95–110.
54. Grandison RC, Piper MDW, Partridge L (2009) Amino-acid imbalance explains extension of lifespan by dietary restriction in *Drosophila*. *Nature* 462(7276):1061–1064.
55. Miller RA, et al. (2005) Methionine-deficient diet extends mouse lifespan, slows immune and lens aging, alters glucose, T4, IGF-I and insulin levels, and increases hepatocyte MIF levels and stress resistance. *Aging Cell* 4(3):119–125.
56. Karabinos A, Schmidt H, Harborth J, Schnabel R, Weber K (2001) Essential roles for four cytoplasmic intermediate filament proteins in *Caenorhabditis elegans* development. *Proc Natl Acad Sci USA* 98(14):7863–7868.
57. McElwee JJ, Schuster E, Blanc E, Thomas JH, Gems D (2004) Shared transcriptional signature in *Caenorhabditis elegans* Dauer larvae and long-lived daf-2 mutants implicates detoxification system in longevity assurance. *J Biol Chem* 279(43):44533–44543.
58. Wood WB (1988) *The Nematode Caenorhabditis elegans* (Cold Spring Harbor Laboratory Press, Cold Spring Harbor, NY).
59. Stiernagle T (2006) in *The C. elegans Research Community, WormBook*, 10.1895/wormbook.1.101.1. Available at www.wormbook.org/chapters/www_strainmaintain/strainmaintain.html. Accessed December 10, 2010.
60. Bogaerts A, Beets I, Temmerman L, Schoofs L, Verleyen P (2010) Proteome changes of *Caenorhabditis elegans* upon a *Staphylococcus aureus* infection. *Biol Direct* 5:11.
61. Braeckman BP, Houthoofd K, De Vreese A, Vanfleteren JR (2002) Assaying metabolic activity in ageing *Caenorhabditis elegans*. *Mech Ageing Dev* 123(2-3):105–119.
62. Brys K, Castelein N, Matthijssens F, Vanfleteren JR, Braeckman BP (2010) Disruption of insulin signalling preserves bioenergetic competence of mitochondria in ageing *Caenorhabditis elegans*. *BMC Biol* 8:91.
63. Wirth M, et al. (2009) HIS-24 linker histone and SIR-2.1 deacetylase induce H3K27me3 in the *Caenorhabditis elegans* germ line. *Mol Cell Biol* 29(13):3700–3709.
64. R Core Team (2013) *R: A Language and Environment for Statistical Computing* (R Foundation for Statistical Computing, Vienna).

Supporting Information

De Haes et al. 10.1073/pnas.1321776111

SI Materials and Methods

Protein Extraction for Two-Dimensional Difference Gel Electrophoresis. Worms were pelleted through centrifugation and washed trice with an isotonic 0.1-M NaCl solution. Live worms were separated from dead worms and remaining bacteria via a density centrifugation step using 30% (vol/vol) sucrose: living worms float on top, whereas dead worms and bacteria pellet out in the sucrose. The live worms were washed three times with an isotonic 0.1-M NaCl solution. The final pellet was added to cold lysis buffer [7 M ureum, 2 M thioureum, 1% DTT, 4% (wt/vol) CHAPS, and 40 mM Tris supplemented with Roche Complete Protease Inhibitor], homogenized, and put on ice. Next, the homogenate was briefly sonicated and then centrifuged for 12 min at 16,000 × *g* (4 °C). Supernatants were desalted overnight at 4 °C using the PlusOne Mini Dialysis Kit (GE Healthcare). Finally, protein concentration in each sample was determined using the Qubit Protein Assay (Invitrogen), and samples were stored at −80 °C until further use.

Trypsin Digestion and Protein Identification. Differential spots were excised using an automated spotpicker (GE Healthcare). Gel plugs were washed with 200 μL ultrapure water for 15 min and subsequently dehydrated by treating them twice with 200 μL 50% (vol/vol) acetonitrile for 15 min. Next the plugs were rehydrated by washing them twice with 100 μL ultrapure water for 5 min. This was followed by a complete dehydration step, in which plugs were submerged in 100 μL 100% (vol/vol) acetonitrile. When the gel plugs were completely white and dehydrated the acetonitrile was removed, and the plugs were allowed to air dry for 10 min. Next, 50 μL of cold digestion buffer [25 mM ammonium carbonate, 5% (vol/vol) acetonitrile] containing 100 ng of sequencing grade modified trypsin (Promega) was added, and the plugs were allowed to swell again at 4 °C. After 30 min we checked whether the gel plugs were still submerged completely and added additional digestion buffer if this was not the case. The plugs were allowed to incubate for 1 additional hour at 4 °C, after which they were incubated at 37 °C overnight. The next day, 100 μL of the first extraction solution [5% (vol/vol) acetonitrile, 5% (vol/vol) formic acid] was added to the digestion buffer, and the plugs were incubated for another 15 min at 37 °C. The solution surrounding a plug, containing the tryptic peptides, was removed and collected in a collection tube. The plugs were resubmerged in 50 μL of the second extraction solution [50% (vol/vol) acetonitrile, 5% (vol/vol) formic acid] and allowed to incubate at 37 °C for 15 s. This solution was added to the same collection tube. The tryptic peptides in each tube were dried using a SpeedVac concentrator (Savant) and subsequently desalted using ZipTip pipette tips (Millipore).

Mass spectrometry was performed on an Ultraflex II MALDI-TOF mass spectrometer (Bruker Daltonics) operated in reflectron positive ion mode. For each spot, 1 μL of tryptic peptides and 1 μL of matrix [saturating amount of α-cyano-4-hydroxycinnamicacid dissolved in 50% (vol/vol) acetone] were spotted on a ground steel MALDI plate (Bruker Daltonics) and allowed to air dry. For each spot, the signal of 3,000 laser shots was added. The instrument was calibrated using *peptide calibration standard II* (Bruker Daltonics). Differential proteins were identified through peptide mass fingerprinting using Mascot (Matrix Science). A mass tolerance of 0.2 Da was used in all searches, and we allowed one missed cleavage per peptide. Carbamidomethylation (C) and oxidation (M) were selected as fixed and variable modifications, respectively. Additionally, all searches were limited to *Caenorhabditis elegans* proteins. We searched the annotated and reviewed SwissProt database for potential identifications. If no clear hit emerged, we additionally searched the general National Center for Biotechnology Information database, because this database contains more sequences (albeit some nonreviewed).

Determining Optimal Concentration of Metformin in Liquid Media. The optimal concentration of metformin in liquid media was determined using a protocol based on the fluorescent dye SYTOX green (Invitrogen). When binding to DNA, SYTOX green emits a green fluorescent signal. However, the dye can only enter cells when their membrane is compromised, thus making it an ideal marker for dead worms (1). In short, worms were synchronized by treating gravid adults with hypochlorite and NaOH. After hatching, L1 worms were transferred to Fernbach flasks containing S medium (2) supplemented with different concentrations of metformin (100 mM, 50 mM, 25 mM, 12.5 mM, 6.25 mM, 0 mM) and constantly shaken. Flash frozen K12 *Escherichia coli* bacteria (Artechno) were added to the cultures as food source until an optimal concentration was reached (OD_{550} = 1.8). The concentration of bacteria was checked twice daily, and new K12 bacteria were added to maintain the cultures at optimal food levels. When worms reached the L4 stage, cultures were supplemented with 2′-deoxy-5-fluorouridine (Sigma-Aldrich) to prevent the formation of progeny (final concentration, 100 mg/L). Once the worms reached the adult stage, samples were taken daily: 190 μL of a worm culture was added to a 96-well plate and mixed with 10 μL of a 20 μM SYTOX green stock solution. After incubating the well plate for 15 min in the dark, dead and living worms were counted using a Leica MZ16F fluorescence microscope. Survival curves were statistically analyzed using a generalized linear model (binomial).

Oil Red O Staining. Worms were fixed in 1× Modified Ruvkun's Witches Brew (MRWB) containing 2% (wt/vol) formaldehyde [made from a 2× MRWB stock: 160 mM KCl, 40 mM NaCl, 20 mM EGTA, 10 mM spermidine, 30 mM Pipes (pH 7.4), and 50% (vol/vol) methanol]. After 1 h, fixed worms were pelleted through centrifugation and washed with S basal. Worms were subsequently incubated for 15 min in a 60% (vol/vol) isopropanol solution, after which the isopropanol solution was replaced with Oil-red O solution [0.3% Oil-red O in 60% (vol/vol) isopropanol]. Worms were rotated in the Oil-red O solution overnight, in the dark. Finally, the stained worms were washed three times with S basal, and bright-field images of the worms were acquired using a Zeiss Axio Imager Z1 microscope. The red component of the Oil-red O images was converted to grayscale and subsequently analyzed using ImageJ. The intensity of Oil-red O staining in each image was acquired using a standardized threshold and normalized against the area of each worm. At least 30 worms were measured for each condition. A Student *t* test was performed to statistically analyze the data.

Electron Micrographs. Nine-day-old adult worms were washed 3 times with 0.1 M NaCl. Worms were subsequently fixed, first in cold 2% (vol/vol) glutaraldehyde, buffered at pH 7.3 with 50 mM Na-cacodylate and 150 mM saccharose, followed by fixation in 2% (wt/vol) osmium tetroxide. Fixed worms were dehydrated in an acetone series and embedded in araldite. Semithin sections of 1 μm cut with a Reichert Ultracut E microtome were stained with methylene blue and viewed in a Zeiss Axioskop light microscope. Double-stained 70-nm thin sections were visualized using a Zeiss EM90 electron microscope.

1. Gill MS, Olsen A, Sampayo JN, Lithgow GJ (2003) An automated high-throughput assay for survival of the nematode *Caenorhabditis elegans*. *Free Radic Biol Med* 35(6):558–565.

2. Stiernagle T (2006) in *The C. elegans Research Community, WormBook* 10.1895/wormbook.1.101.1. Available at www.wormbook.org/chapters/www_strainmaintain/strainmaintain.html. Accessed December 10, 2010.

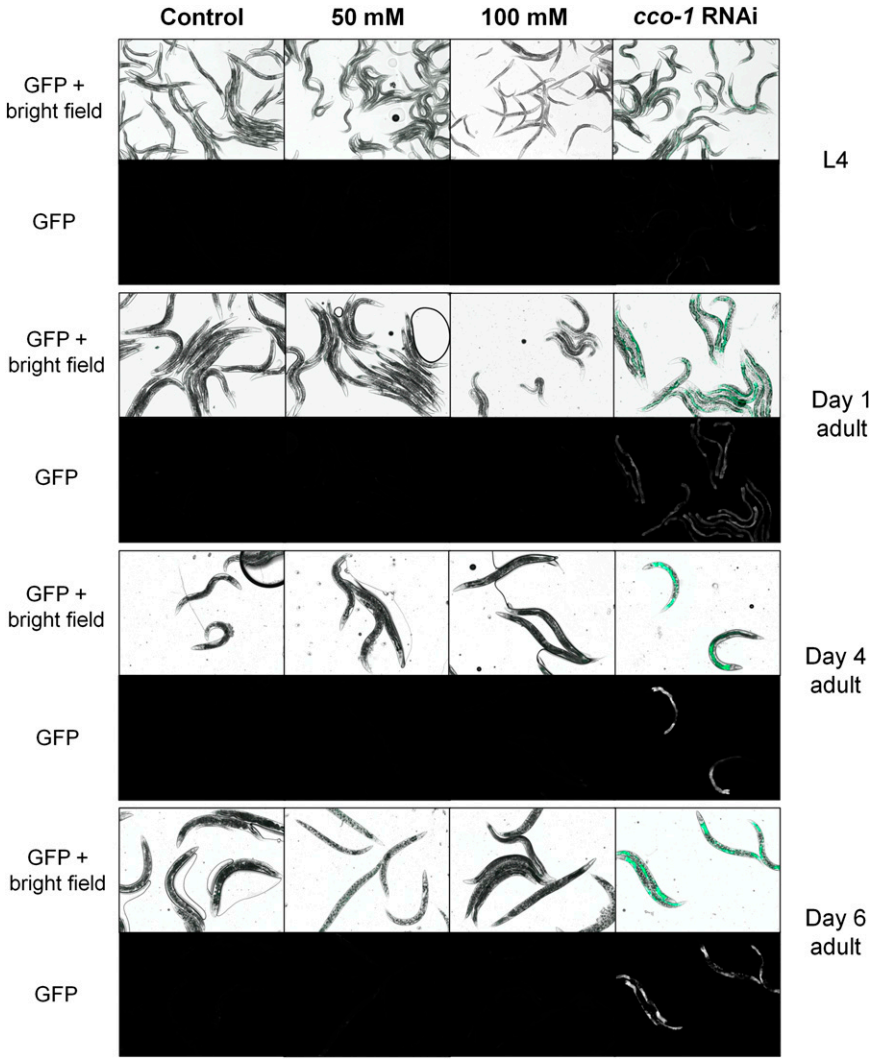

Fig. S1. Metformin treatment does not induce the mitochondria-specific unfolded protein response. Metformin-treated *hsp-6*::GFP worms show no difference in fluorescence compared with untreated control worms, both at the optimal concentration of 50 mM and at a higher concentration (100 mM), indicating that metformin-mediated lifespan extension via the induction of the UPR^{mt} is highly unlikely. *hsp-6*::GFP worms were exposed to *cco-1* RNAi as a positive control, which resulted in a marked increase in fluorescence, especially after the L4 stage. *cco-1* encodes a cytochrome *c* oxidase subunit, an integral part of the mitochondrial electron transport chain (1).

1. Durieux J, Wolff S, Dillin A (2011) The cell-non-autonomous nature of electron transport chain-mediated longevity. *Cell* 144(1):79–91.

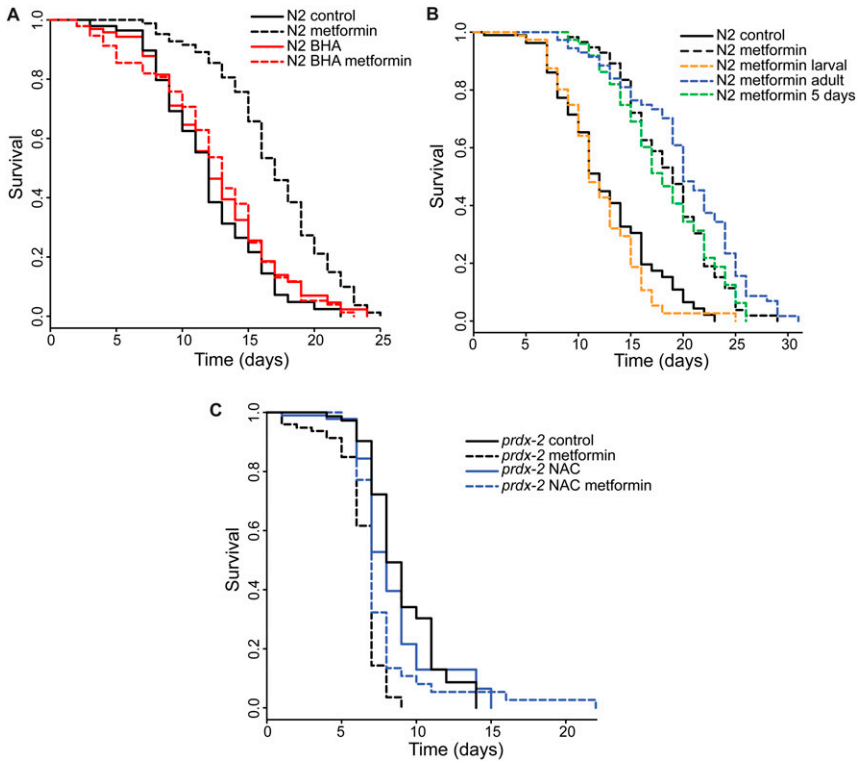

Fig. S2. Diverse lifespan experiments. (*A*) Treatment with the fat-soluble antioxidant butylated hydroxyanisole (BHA) abolishes the lifespan extending effect of metformin (***$P < 0.001$; $n \geq 97$ for each curve; Table S1). (*B*) Metformin exposure restricted to adulthood or to the first 5 d of adulthood is sufficient to extend lifespan (***$P < 0.001$ for both). Limiting metformin exposure to the larval stages had no significant effect on longevity ($^{n.s.}P > 0.05$; $n \geq 92$ for each curve; Table S1). (*C*) The antioxidant *N*-acetylcysteine (NAC) partially rescues the debilitating effect of metformin on *prdx-2* knockout worms (***$P < 0.001$; $n \geq 90$ for each curve; Table S1).

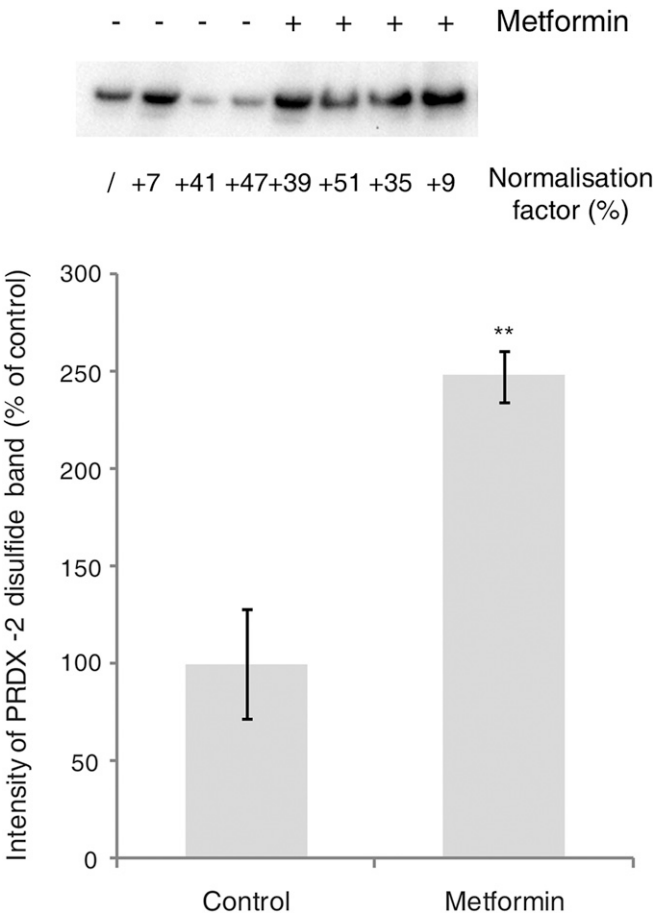

Fig. S3. Metformin treatment induces formation of PRDX-2 dimers. Nonreducing Western blot was performed to quantify the amount of oxidized PRDX-2 dimers after metformin treatment (50 mM). Band intensity was normalized against total protein content in each lane and plotted in a bar graph. The normalization factor is acquired by referencing the amount of protein in the first lane to the total protein ratio for each other lane. The bar graph shown is the same graph as Fig. 2*E* in the main text. Bars represent mean ± SEM ($n = 4$).

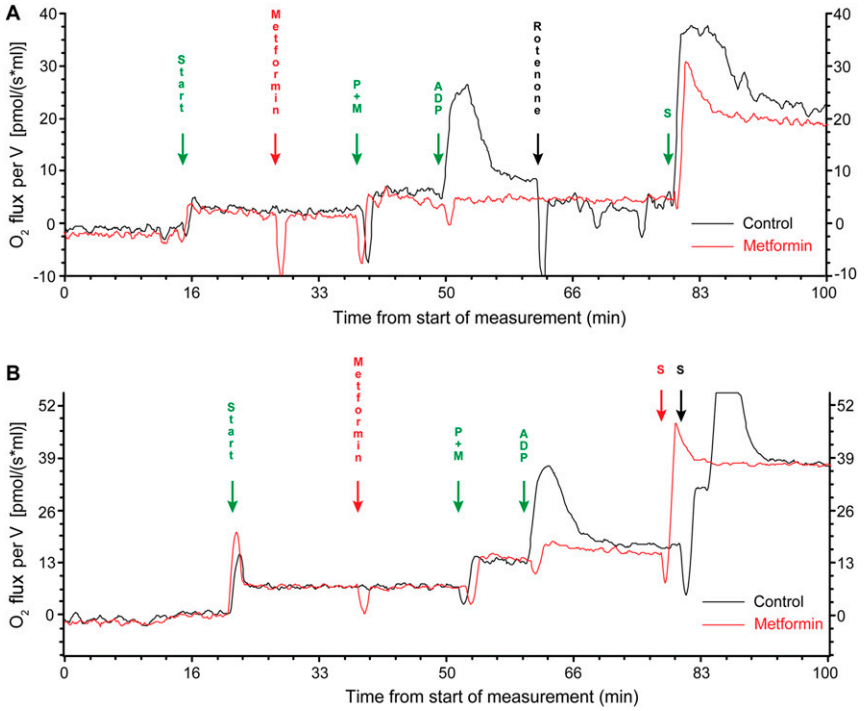

Fig. S4. Metformin inhibits complex I of the mitochondrial electron transport chain (ETC). (*A*) Metformin and rotenone inhibit complex I- but not complex II-based respiration. The effect of metformin on mitochondrial respiration was measured by sequentially adding compounds to stimulate different parts of the ETC. A positive O_2 flux indicates the use of oxygen by mitochondrial respiration, with higher values indicating higher respiration, negative values indicating a small influx of O_2, usually due to the injection of a compound. Green arrows indicate compounds that were added in both the control and metformin-treated cell; red and black arrows indicate compounds that were only added in the treated or control cell respectively. After adding an equal volume of mitochondria (↓start), metformin was added to one of the cells (↓metformin). Subsequently, the complex I substrates pyruvate and malate (↓P+M) were added, followed by the addition of ADP (↓ADP), thus initiating electron transport from complex I. In the control cell respiration clearly increased, whereas the metformin-treated mitochondria failed to initiate complex I-based respiration, thus indicating that metformin inhibits electron transport from complex I in vitro. Because of the higher concentration of mitochondria and a resultant depletion of substrates, this peak was more transient than in Fig. 3*A*. Subsequently, we inhibited complex I-based respiration in the control cell using rotenone (↓rotenone), resulting in a drop in respiration to the baseline. Finally, the complex II substrate succinate (↓S) was added to both cells, which led to a marked increase in mitochondrial respiration, thus indicating that metformin and rotenone did not block electron transport from complex II. (*B*) Similar setup as previously described, except no rotenone was added and succinate (↓S) was added to both cells, revealing a cumulative effect of complex I and II respiration in the control cell.

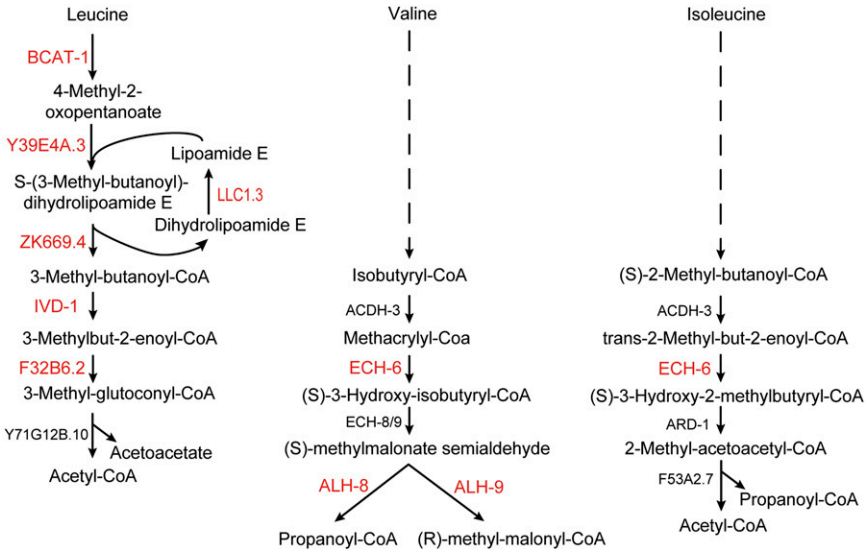

Fig. S5. Metformin treatment induces the branched-chain amino acid (BCAA) degradation pathway. The BCAA degradation pathway, based on the BCAA pathway from the Kyoto Encyclopedia of Genes and Genomes. Enzymes noted in red are up-regulated after metformin treatment. The same enzymes are used in the first steps of the degradation of each BCAA (dashed line).

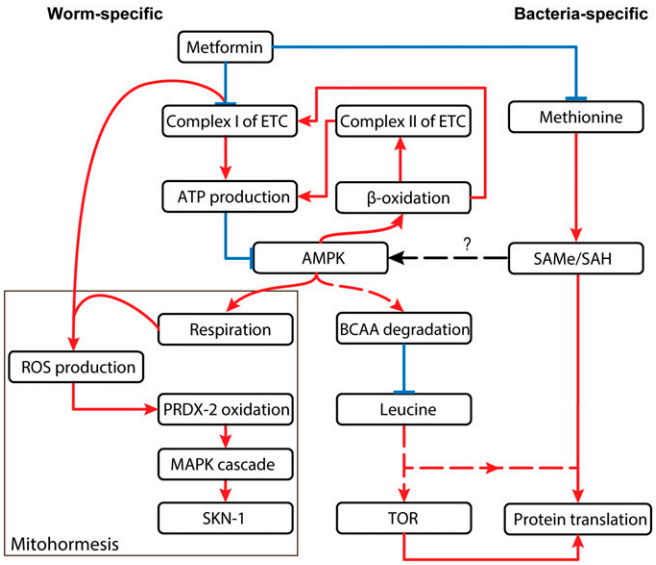

Fig. S6. Putative mode of action for metformin-mediated lifespan increase. Scheme summarizing the different effects of metformin in *C. elegans*. Blue lines represent a negative or inhibitory effect; red lines represent positive or stimulatory effect. The direct effect of metformin is thoroughly described in this article. For more information about the bacteria-specific effect of metformin, see Cabreiro et al. (1). In summary, metformin inhibits complex I of the ETC in a way distinct from the classic complex I inhibitor rotenone, causing increased ROS production. This inhibition leads to a decrease in ATP levels and a resultant activation of AMPK, leading to an increase in catabolism and respiration, which in turn exacerbates the metformin-mediated production of ROS. The increased production of ROS activates the mitohormetic pathway through oxidation of PRDX-2 (Fig. 6 gives more detail on the metformin-mediated induction of mitohormesis). Simultaneously, an increase in activity in the BCAA degradation pathway causes a reduction in BCAA (leucine, valine, and isoleucine) concentration. It is, however, unknown how metformin is able to induce increased BCAA degradation. To our knowledge, there is no evidence of AMPK as being directly involved in BCAA degradation. Present knowledge of the BCAA degradation pathway in mammals indicates that it is mainly activated by the group of peroxisome proliferator-activated receptors, which in turn are activated by free fatty acids and other fatty acid derivatives (2). Because AMPK activates lipases in adipose tissues and thus increases the concentration of these free fatty acid ligands (3), the kinase may yet be indirectly involved in the activation of the BCAA degradation pathway. We speculate that this activation leads to reduced protein translation both indirectly through inhibition of TOR and directly through a reduction of substrate available for protein translation. The combination of mitohormesis and reduced protein translation adds to an increased healthspan.

1. Cabreiro F, et al. (2013) Metformin retards aging in *C. elegans* by altering microbial folate and methionine metabolism. *Cell* 153(1):228–239.
2. Harris RA, Joshi M, Jeoung NH (2004) Mechanisms responsible for regulation of branched-chain amino acid catabolism. *Biochem Biophys Res Commun* 313(2):391–396.
3. Kahn BB, Alquier T, Carling D, Hardie DG (2005) AMP-activated protein kinase: ancient energy gauge provides clues to modern understanding of metabolism. *Cell Metab* 1(1):15–25.

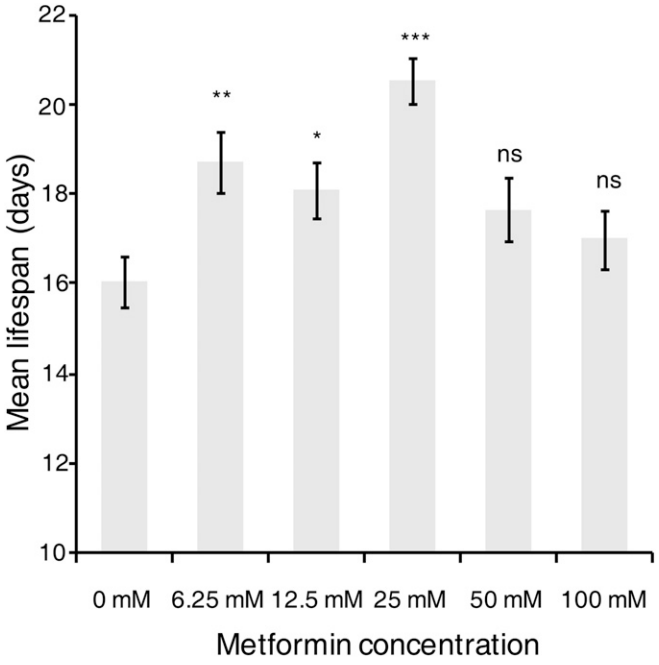

Fig. S7. Effect of metformin on *C. elegans* lifespan in liquid media. Graph showing the mean lifespan of *C. elegans* in liquid media after treatment with different concentrations of metformin. Lifespan extension reached an optimum at 25 mM of metformin (***$P < 0.001$). Bars represent mean life span ± SEM.

Table S1. Summary of performed lifespan experiments

Condition	N	#	Mean LS	± SEM	Effect of metformin (%)	*p*LogRank	*p*COXPH
Experimental group 1: control vs. *prdx-2* and NAC							
N2	172	10	12.79	0.43	30.57	1.48E-9***	NA
N2 Met	169	10	16.70	0.40			
prdx-2	139	10	10.61	0.40	−36.27	6.00E-16***	< 2E-16***
prdx-2 Met	127	10	6.76	0.18			
N2 NAC	171	10	13.17	0.49	5.54	0.419 ns	6.40E-4***
N2 NAC + Met	171	10	13.90	0.48			
Experimental group 2: control DMSO vs. BHA							
N2 DMSO	99	5	11.99	0.55	40.78	2.48E-09	NA
N2 DMSO + Met	97	5	16.88	0.45			
N2 BHA	99	5	12.52	0.64	−0.005	0.898 ns	7.54E-5***
N2 BHA + Met	101	5	12.45	0.54			
Experimental group 3: metformin timings							
N2	97	5	12.65	0.63	NA	NA	NA
N2 Met	92	5	18.65	0.58	47.43	3.95E-9***	NA
N2 Met adult	102	5	19.90	0.57	57.31	1.22E-12***	NA
N2 Met 5 d	98	5	18.21	0.63	43.95	3.95E-9***	NA
N2 Met larval	99	5	12.06	0.60	−0.046	0.502 ns	NA
Experimental group 4: NAC and *prdx-2* interaction							
prdx-2	90	5	8.79	0.30	−27.19	2.62E-11***	NA
prdx-2 Met	99	5	6.40	0.17			
prdx-2 NAC	98	5	8.49	0.45	−8.95	0.084 ns	2.15E-5***
prdx-2 NAC+Met	98	5	7.73	0.38			
Experimental group 5: control vs. acdh-1							
N2	75	5	12.95	0.60	13.67	0.013*	NA
N2 Met	77	5	15.00	0.49			
acdh-1	85	5	9.03	0.41	76.52	7.33E-10***	8.21E-9***
acdh-1 Met	54	5	15.94	0.86			

The total amount of tested worms (N), the number of independent experiments (#), the mean lifespan (mean LS with error), and the increase in mean lifespan due to metformin treatment are shown for each tested strain or condition. Both log–rank and Cox proportional hazard tests were performed to determine statistical significance. *p*LogRank is the *P* value of the log–rank test used to compare survival between treated and nontreated worms within a single strain, corrected for multiple testing (Benjamini-Hochberg). *p*COXPH is the *P* value of the Cox proportional hazard test used to determine whether the effect of metformin was different from the effect of metformin on the control. ns, not significant; *$P < 0.05$; ***$P < 0.001$.